AGU PUBLICATIONS

JGR

Journal of Geophysical Research: Earth Surface

RESEARCH ARTICLE
10.1002/2014JF003100

Key Points:
- Meltwater refreezing across ice caps simulated from new field-calibrated model
- Application to Devon Ice Cap reproduces patterns of observed snow facies
- Runoff very sensitive to temperature as warmer firn has low refreezing capacity

Correspondence to:
D. W. F. Mair,
d.mair@abdn.ac.uk

Citation:
Morris, R. M., D. W. F. Mair, P. W. Nienow, C. Bell, D. O. Burgess, and A. P. Wright (2014), Field-calibrated model of melt, refreezing, and runoff for polar ice caps: Application to Devon Ice Cap, *J. Geophys. Res. Earth Surf.*, *119*, 1995–2012, doi:10.1002/2014JF003100.

Received 24 JAN 2014
Accepted 29 JUN 2014
Accepted article online 1 JUL 2014
Published online 29 SEP 2014

Field-calibrated model of melt, refreezing, and runoff for polar ice caps: Application to Devon Ice Cap

Richard M. Morris[1], Douglas W. F. Mair[1], Peter W. Nienow[2], Christina Bell[3], David O. Burgess[4], and Andrew P. Wright[5]

[1]School of Geosciences, University of Aberdeen, Aberdeen, UK, [2]School of Geosciences, University of Edinburgh, Edinburgh, UK, [3]Scottish Natural Heritage, Fort William, UK, [4]Natural Resources Canada, Ottawa, Ontario, Canada, [5]Department of Geography, University of Exeter, Exeter, UK

Abstract Understanding the controls on the amount of surface meltwater that refreezes, rather than becoming runoff, over polar ice masses is necessary for modeling their surface mass balance and ultimately for predicting their future contributions to global sea level change. We present a modified version of a physically based model that includes an energy balance routine and explicit calculation of near-surface meltwater refreezing capacity, to simulate the evolution of near-surface density and temperature profiles across Devon Ice Cap in Arctic Canada. Uniquely, our model is initiated and calibrated using high spatial resolution measurements of snow and firn densities across almost the entire elevation range of the ice cap for the summer of 2004 and subsequently validated with the same type of measurements obtained during the very different meteorological conditions of summer 2006. The model captures the spatial variability across the transect in bulk snowpack properties although it slightly underestimates the flow of meltwater into the firn of previous years. The percentage of meltwater that becomes runoff is similar in both years; however, the spatial pattern of this melt-runoff relationship is different in the 2 years. The model is found to be insensitive to variation in the depth of impermeable layers within the firn but is very sensitive to variation in air temperature, since the refreezing capacity of firn decreases with increasing temperature. We highlight that the sensitivity of the ice cap's surface mass balance to air temperature is itself dependent on air temperature.

1. Introduction

Summer air temperatures over polar ice masses are predicted to continue rising throughout the next century [*Meehl et al.*, 2007]. Efforts to deduce the effect of this rise on runoff, and hence mass balance, must consider meltwater refreezing and retention, else runoff will be overestimated significantly [*Bougamont et al.,* 2007; *Janssens and Huybrechts,* 2000; *Pfeffer et al.*, 1991]. Uncertainty in the amount of runoff increases into the future as melt extent and duration change further. Previous studies have quantified the importance of meltwater retention and its impact on mass balance. *Wright et al.* [2007] showed that at Midre Lovénbreen in Svalbard the inclusion of refreezing within mass balance calculations could counteract the effect on runoff of increasing air temperature at the rate of 0.1°C per decade, while at the scale of the Greenland Ice Sheet, *Pfeffer et al.* [1991] estimate that neglecting refreezing could lead to an overestimation in runoff of around 4 cm of sea level rise over the next 150 years.

The quantification of meltwater refreezing is also important for the interpretation of remote sensing data sets. Satellite radar altimetry has long been used to observe the surfaces of large ice masses [e.g., *Partington et al.*, 1989], since by measuring surface elevation change across the dry snow zone, annual accumulation can be inferred by assuming or measuring a value for surface density. Across the rest of the accumulation zone, however, the refreezing of meltwater to form ice layers within the near-surface stratigraphy has a strong effect on the surface and near-surface reflectivity to radar waves, introducing a substantial uncertainty to the altimetry method [*Scott et al.*, 2006]. A further complication lies in the conversion of elevation changes to mass changes, for which knowledge of any subsurface density change is required [*Brathwaite et al.*, 1994]. Many previous models deal with dry densification [*Herron and Langway*, 1980; *Zwally and Li*, 2002] or wet densification that allows meltwater to refreeze within the same annual layer in which it is created [*Reeh et al.*, 2005]. However, percolation of meltwater into the firn of previous years, known as internal accumulation, may also be important. Better knowledge of the spatial and temporal variations in near-surface refreezing of meltwater within the snow and firn will reduce the uncertainty in altimetry products due to these complications.

Large-scale parameterizations of meltwater refreezing and retention have been developed to investigate the effect of refreezing on mass balance and to predict the sensitivity of ice sheets to future climate change [*Van Angelen et al.*, 2013]. *Janssens and Huybrechts* [2000] presented four simple snowpack retention schemes suitable for incorporation into large-scale ice sheet models. Their schemes produced similar total amounts of meltwater retention and runoff, but with the more complex, more physically based parameterizations showing a much larger spatial variation. This is in contrast to the results of *Bougamont et al.* [2007] who showed that more detailed schemes allow more refreezing and are more sensitive to climate change. Modeling carried out by *Van den Broeke et al.* [2008] on the K-transect, at 67°N in west Greenland shows the variation in meltwater retention with altitude, with an insignificant amount at the lowest elevations but over 90% in the middle of the ablation zone. The various modeling studies do not agree on the sensitivity of refreezing to climate. This is in part because of uncertainties in the most important refreezing processes but is also due to the lack of in situ observational data against which to calibrate and validate models. Consequently, model comparison exercises have limited themselves to discussion of the consistency of results from different models [*Bougamont et al.*, 2007; *Reijmer et al.*, 2012]. Thus, there is a need for models of refreezing and runoff to be calibrated and validated against in situ field observations. Furthermore, since there is a strong spatial variability in refreezing and retention, if models are to be extrapolated across ice sheets and transferrable across different ice masses, they should be tested against measurements spanning a wide range of snow facies and meteorological conditions.

This paper aims to address these inadequacies by modifying a physically based model that simulates the evolution of the snow and near-surface firn and applying it to an ice cap where detailed snow and firn measurements are available across the range of snow facies, at the start and end of two summer melt seasons. The model is calibrated using the field measurements in 1 year, validated against measurements from another, and the sensitivity of the model to internal and external controls is examined. We model changes in the thermal structure and density profile of the snowpack at high vertical resolution so that the surface extents of the different accumulation zone facies (i.e., dry snow zone, percolation zone, and wet snow zone) [*Benson*, 1962] can be defined each summer for which the model is run. The model output predicts the amounts of melting, refreezing within the snow and near-surface firn, and runoff over the season, allowing a calculation of mass balance that includes the effect of internal accumulation.

In this paper, we first describe the model and its modifications for this work, before outlining its calibration with data from Devon Ice Cap (DIC) in Arctic Canada. Results for the calibration and validation periods are shown for a range of spatial scales, and the sensitivity of the model to changes in the internal stratigraphy of the snow and firn and to air temperature are shown. We finish with a discussion of these results and their implications within the context of previous work.

2. Model Description

2.1. Summary

Our model has its origins in the work of *Greuell and Konzelmann* [1994]. Their model, applied to the Greenland Ice Sheet, was later adapted for application to the Academy of Sciences Ice Cap, Russian High Arctic [*Bassford*, 2002], and to Midre Lovénbreen, Svalbard [*Wright*, 2005]. We now outline the main components of the model, detailing some of its assumptions and simplifications, before highlighting the modifications we have made that differ from previous applications.

The model calculates time-evolving energy and mass balance for a series of points down a linear transect, based on a small number of input measurements and specified parameters. At each point the model consists of a one-dimensional vertical grid representing the surface snowpack and the firn (or ice) underneath.

The surface energy balance [*Hock*, 2005],

$$Q_t = G(1-\alpha) + L + Q_h + Q_l, \tag{1}$$

is solved by evaluating each factor in turn using weather station data and parameterizations. Q_t, Q_h, and Q_l are the total surface, sensible, and latent heat fluxes respectively (W m^{-2}); G is global solar radiation (W m^{-2}); α is the surface albedo; and L is the longwave radiation balance (W m^{-2}). Q_t, the surface heat flux, combines the energy used for surface temperature change and melt, and heat energy conducted to/from the subsurface. Fluxes toward the surface are positive. The calculation of the surface energy balance requires

three variables as input: air temperature, global (incoming solar) radiation, and relative humidity. These meteorological data are available at hourly resolution and were downscaled to the model time step of 15 min.

The surface mass change is calculated by determining accumulation, melt (driven by energy balance), and runoff. The density and temperature profiles at each point evolve over the model run. This occurs in three stages: the addition of accumulation, the generation of meltwater, and the adjustment of the subsurface density and temperature profiles, taking account of refreezing and thermal conduction of heat.

Time series of accumulation from weather stations (again, available at hourly resolution and downscaled to match the model time step of 15 min) are combined with user-defined lapse rates for precipitation and air temperature, considered to be taken at a reference height of 2 m ($T_{2\ \mathrm{m}}$) to calculate an accumulation record at each grid point. A threshold air temperature, compared to $T_{2\ \mathrm{m}}$, determines whether measured accumulation is in the form of snow or rain. Snowfall is added to the top of the grid, whereas rainfall immediately begins to percolate downward through it. Added snowfall causes the top grid cell to thicken (while melting causes it to thin). Fresh snow takes the density of ρ_s, and the bulk density of the top cell is modified to incorporate the new material. The amount of snow/firn converted to meltwater is based on the integral of Q_t (equation (1)) over the 15 min model time step. Q_t first raises the surface temperature to the melting point and then causes the generation of melt.

The final part of the model deals with the percolation and refreezing of meltwater and thermal conduction between cells and the effects these processes have on the density and temperature profiles. The refreezing process is dealt with first. Liquid water, from both melting and rainfall, percolates downward through the grid, refreezing within each cell until either the density of the cell reaches that of ice, or the latent heat release from the refreezing balances the cold content in the cell, so that it is warmed to the melting point. The model then calculates the modification to T, the vertical temperature profile of the grid (K), due to latent heat release from refreezing meltwater. The model attempts to achieve a balance between accuracy and simplicity, and therefore, some processes are omitted. In particular, the model simplifies the mechanics of water percolating through a snowpack, e.g., by assuming matrix flow and neglecting the rapid transfer of water downward without refreezing by "finger flow" [*Campbell et al.*, 2006].

2.2. Model Modifications

Bassford et al. [2006] and *Wright et al.* [2005] used a vertical grid cell size of 5 cm for all material above glacier ice then allowed cell size to increase exponentially with depth, with the lowest cell given a vertical size of around 2 m. This was undertaken so that density and temperature profiles would have the highest resolution close to the surface, where temporal and spatial gradients are strongest, while calculations could be carried out to depth without compromising computational efficiency. However, the percolation and refreezing of meltwater often creates ice lenses and layers with thicknesses on the order of 1 cm or less [e.g., *Bell et al.*, 2008]. Thus, in an attempt to improve the ability of the model to simulate different accumulation zone facies, our model sets the vertical grid cell size to 1 cm for all cells. To offset the increased computational time, the grid is not extended to the 20–25 m depth below the base of the snowpack employed by previous model versions [*Bassford et al.,* 2006; *Greuell and Konzelmann,* 1994; *Wright et al.*, 2005] but extends initially only to a depth of 3 m into the firn below the snowpack so that calculations are quickened. Three meters was chosen as it was the smallest whole number of meters that provided enough depth that all of the measured impermeable layer depths could be incorporated into the model. Preliminary tests showed that the thermal evolution of the snow and firn above the impermeable layer was not dependent on the depth of the model grid, with a negligible change when the grid depth was varied up to 30 m.

Surface albedo is calculated as a function of the density of the top 10 cm of the grid in a similar manner to that of *Greuell and Konzelmann* [1994], but without the dependency on cloud cover as cloud data were unavailable. In our calculations of the longwave radiation balance, the atmospheric emissivity, ε, is calculated; thus,

$$\varepsilon = 1.72 \times \left(1000 \frac{e}{T_{2\ \mathrm{m}}}\right)^{\frac{1}{7}} \times \left(1 + 0.22c^2\right) \tag{2}$$

where c is the fractional cloud cover, given a constant value (see section 4.1), and e is the atmospheric water vapor pressure (Pa), calculated following *Oerlemans* [1992]. This formulation was developed for use with DIC by A. Gardner (personal communication, 2010) and is based on *Brutsaert* [1975] and *Kustas et al.* [1994].

Our model uses Q_t to modify the temperature of the top grid cell only. It is therefore simpler than the method of *Greuell and Konzelmann* [1994], which divided *G* into surface-absorbed (36%) and subsurface-absorbed (64%) components, with the subsurface component absorbed at depth within the grid according to an exponential function. The reasoning behind this simplification is that the wavelengths of solar radiation that are absorbed by snow are absorbed within the top few millimeters, while more deeply penetrating wavelengths are scattered back to the surface [*Brandt and Warren,* 1993]. Since the top cell always has a vertical extent of at least 1 cm, our model simplifies the calculation by allowing only this top grid cell to interact with the atmosphere through the surface energy balance. *Bugnion and Stone* [2002] and *Van den Broeke et al.* [2008] use the same simplification for a snow surface.

The original model version [*Greuell and Konzelmann,* 1994] was applied to a single point, while further work [*Bassford et al.*, 2006; *Wright et al.*, 2005] applied the model to a grid or flow line of points. We also apply the model to sets of points, along which field data have also been collected.

3. Data

We applied the model to the Cryosat calibration/validation transect of DIC (Figure 1). Measurements used to run the model are presented in *Bell et al.* [2008]. Detailed stratigraphic logging of snowpack structure and density was carried out at ~1 km intervals along a 47 km transect over an elevation range between ~480 m and ~1800 m above sea level (asl), in the spring (premelt) and autumn (during/after melt) of 2004 and 2006. Measurements characterize the seasonal snowpack variability across the full spectrum of surface facies between the percolation and ablation zones [*Benson*, 1962]. The spring data characterize the snow/firn before the summer melt, and the autumn data characterize the metamorphosed snow/firn following summer melt, percolation, and refreezing processes. At each site (numbering 38 in 2004 and 37 in 2006; Figure 1), snowpits were dug down to the surface layer demarcating the end of the previous summer. This layer was easily identified as a hard, icy, and continuous layer located beneath the autumn hoar and was used as a reference surface for the bottom of each year's snowpits. Once this layer was identified in spring, ablation stakes were emplaced and used as markers to ensure this same horizon was used as a common reference for any depth change identified upon remeasurement in the following autumn. Standard snowpit stratigraphic procedures were followed [*Colbeck et al.*, 1990]. Snowpit stratigraphy, density, grain size, grain type, hardness, and temperature were logged on north facing pit walls. Density measurements involved weighing a sample of known volume (100 cm^3) from each stratigraphic layer. *Harper and Bradford* [2003] found that measurement errors associated with this type of density sampling were 10%. In spring seasons, pits were dug at 1 km intervals along the full length of the transect. In autumn seasons, pits were dug as far along the length of the transect as was possible owing to snowpack removal, saturation, or time constraints of digging pits dominated by thick (>10 cm) ice layers at lower elevations. These ice features were allocated a density of 800 kg m^{-3} since it was not possible to measure their density directly in the field, and the ice was often observed to contain bubbles [see *Bell et al.*, 2008, Figures 9 and 10].

Automated weather stations (AWSs) were set up along the transect in spring 2004 at 1801 m asl and 1415 m asl. Combined with 15 HOBO temperature data loggers, spaced approximately every 3 km, these measured temporal and spatial variation in air temperatures ($T_{2\ m}$) along the transect. The AWS also measured relative humidity (*H*) and incoming solar radiation (*G*). Ultrasonic depth gauges on the AWS measured changes in surface height, from which time series of accumulation were calculated. The temperature and accumulation records were used to calculate lapse rates used to extend the measurements across the entire transect.

4. Model Application

Vertical grids of 1 cm resolution were initialised at each point for which spring snow and firn data were available. For the snow portion of each grid, a density stratigraphy was based directly on measurements taken at each site. The thermal profile at each site was determined from sets of temperature measurements with 10 cm vertical resolution, collected at the two AWS sites and at each snowpit site below 1415 m asl (24 sets of measurements in total for 2004, 22 for 2006). Gaps in the data sets were filled by altitude-based linear interpolation between known profiles. The firn portion of each grid was based on less detailed data. The depth of the uppermost impermeable layer within the firn of each grid was assigned using the firn core taken at each point. Impermeable layer depths were taken as equal to the top surface of the uppermost ice layer that exceeded 5 cm thickness

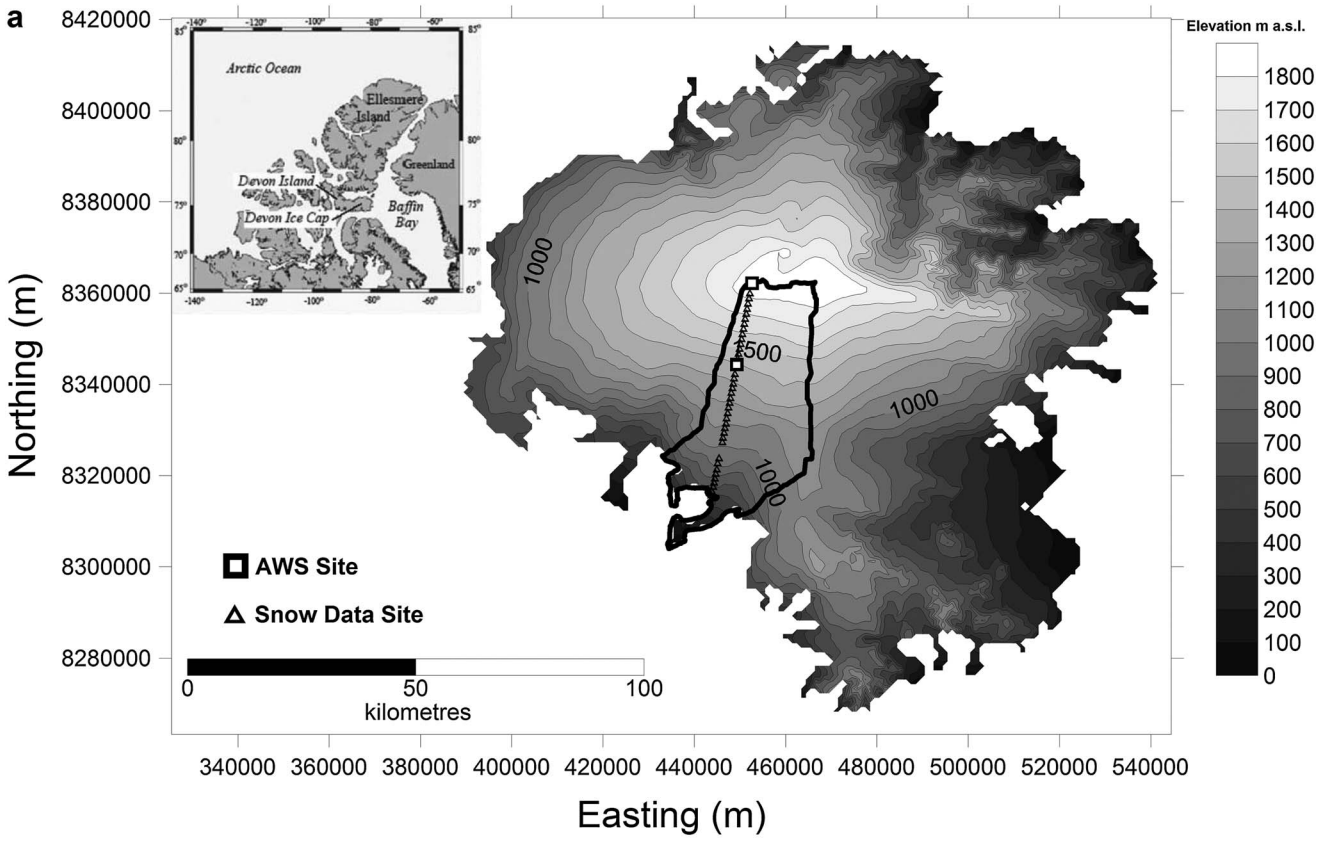

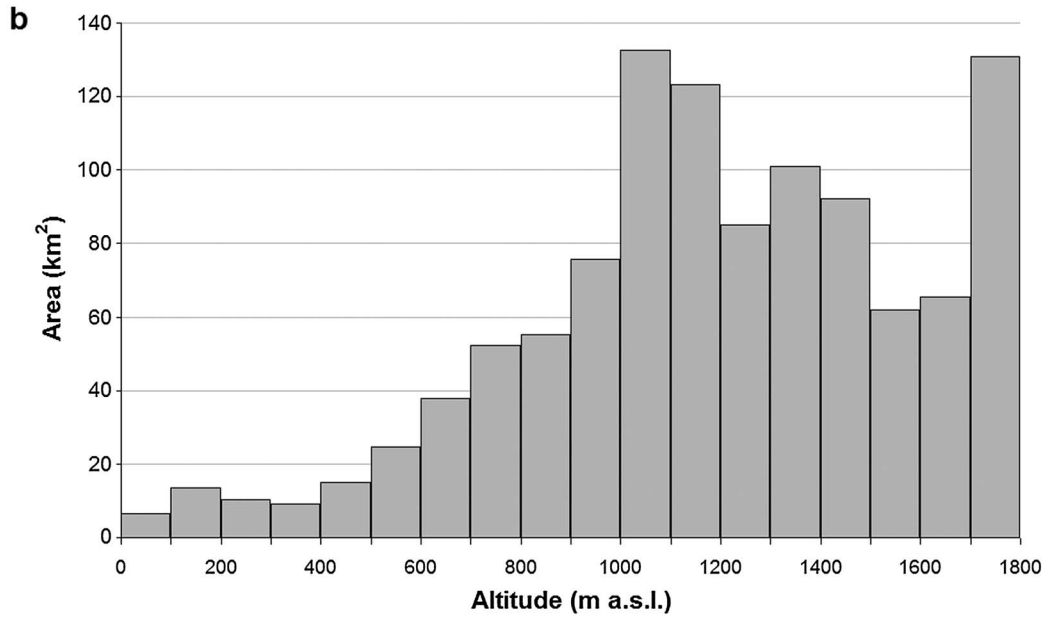

Figure 1. (a) Digital elevation model of Devon Ice Cap (DIC), showing data collection sites. Inset shows position of DIC within the Queen Elizabeth Islands of arctic Canada. Automatic weather stations used in this study are shown by squares and snow data collection sites by triangles. The outline of basin 40 [*Burgess and Sharp,* 2004] is also shown by a thick black line. Coordinates are universal time meridian (zone 17). (b) Catchment hypsometry for DIC basin 40, averaged for 100 m elevation bands [from *Burgess and Sharp*, 2004].

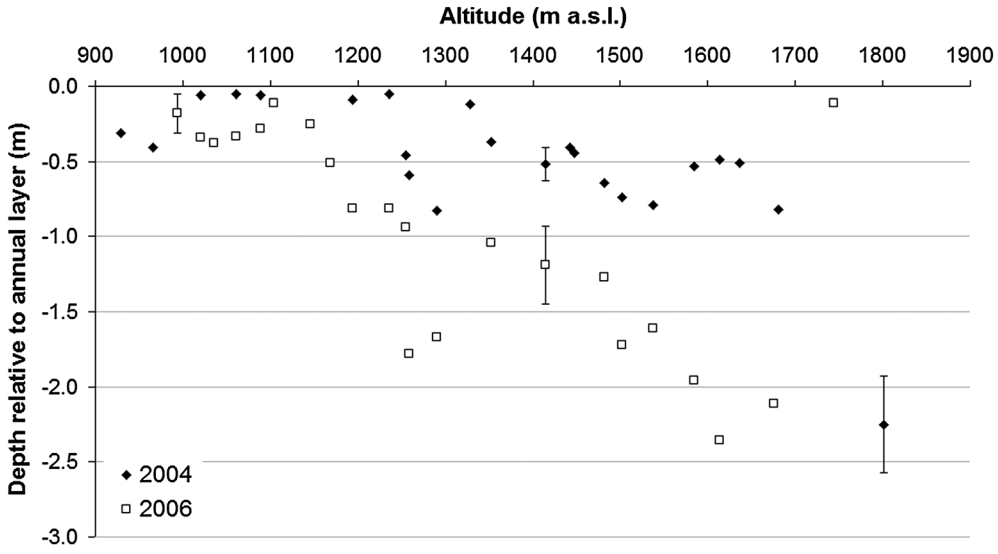

Figure 2. Uppermost impermeable layer depth found at each site, in both years of measurement. Error bars at certain sites show kilometer-scale spatial variability, based on 1 km^2 nested grids.

within each firn core (Figure 2). The firn density profile was created by giving all cells above the impermeable layer a density value of 550 kg m^{-3}, the average density of the firn across all cores (to the nearest 50 kg m^{-3}), and all below a value equal to the density of ice, ρ_i. Firn temperature profiles were based on the theoretical profiles presented in *Paterson* [1994, p. 206], calculated for the two AWS sites, and an altitude-based lapse rate applied to calculate profiles for each grid.

4.1. Model Calibration and Validation

The data from the 2004 melt season were used to calibrate the model, which requires a number of user-defined parameters. These parameters, shown in Table 1, were not constrained by data. Therefore, a strategy was devised to determine which of these parameters were the most important, and their optimal values. The first part of this strategy used a systematic equidistributed sample of the five-dimensional parameter space defined in Table 1, and the second part used a Monte Carlo simulation.

4.1.1. Systematic Sample Phase

The model was run repeatedly using each combination of the parameter values shown in Table 1. Since each parameter has nine possible values, the total number of model runs in this phase was 9^5. The model output for each run was compared with end-of-season measurements of snowpack water equivalent, height, and bulk density. Normalized root-mean-square deviation (NRMSD) between model and measured values of each of these three measurements were averaged to calculate a "goodness-of-fit" measure of the accuracy with which the model run fit the data.

By observing the change in the goodness-of-fit measure caused by varying the snow-rain threshold temperature and fractional cloud cover, we found the model to be insensitive to change in either of these parameters. The model is most accurate using a value for the snow-rain threshold air temperature of between 0.4°C and 1.5°C, but within that range precise selection matters little. Therefore, a value of 1°C was chosen. *Bassford* [2002] used a value of 0°C on the Vavilov ice cap, and *Wright* [2005] used 1.6°C for Midre Lovénbreen. This range of values

Table 1. Parameters Used in Calibration of Model, With Bounds of Searched Parameter Space Shown, and Step Used for Systematic Search

Name	Symbol	Bounds	Step	Unit
Albedo (fresh snow)	α_s	0.76–0.88	0.015	
Albedo (ice)	α_i	0.41–0.65	0.03	
Density (fresh snow)	ρ_s	280–440	20	kg m^{-3}
Snow-rain threshold temperature		−0.5–1.9	0.3	°C
Cloud cover	c	0.1–0.9	0.1	

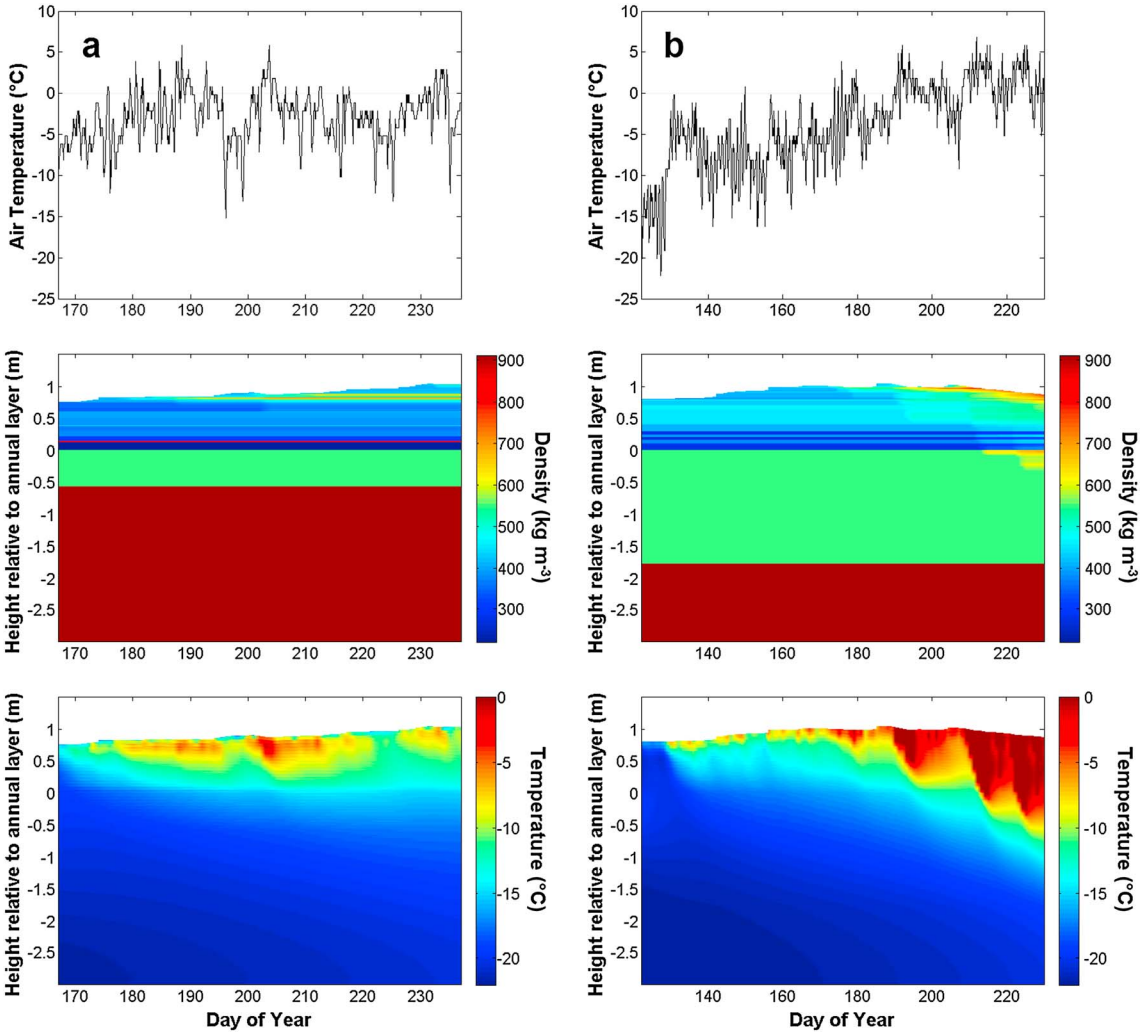

Figure 3. (top) Time series of air temperature (°C), alongside contour graphs showing the evolution of (middle) the density stratigraphy (kg m^{-3}), and (bottom) the thermal profile (°C) for a site on the transect at 1259 m asl in (a) 2004 and (b) 2006.

illustrates the fact that the value chosen is a parameterization of many processes acting at the local scale. The model is most accurate when a value for cloud cover between 10% and 40% is used, and again, variation within these bounds makes little difference. Therefore, a value of 33% was selected, based on an estimate of the overall average during fieldwork. The model was found to be much more sensitive to the three other parameters from Table 1, namely, the density of fresh snow (ρ_s) and the albedos for snow and ice (α_s and α_i, respectively). These were optimized during the second phase of model optimization.

4.1.2. Monte Carlo Phase

A 1000 run Monte Carlo simulation was used to find optimal values for ρ_s, α_s, and α_i. Values for these three parameters were randomly drawn for each run from independent rectangular (uniform) distributions with bounds as shown in Table 1. As for the systematic phase, the NRMSD between modeled and measured values of three output variables (snowpack water equivalent, height, and bulk density) were averaged for each run, in order to quantify the goodness of fit. The optimal values found (together giving the run with the lowest average NRMSD) for ρ_s, α_s, and α_i were 0.41, 0.81, and 0.65, respectively.

4.1.3. Validation

The model was validated by running it for the 2006 melt season with the same parameter set that was calibrated to the 2004 season. Year 2006 was substantially warmer than 2004: average air temperature during the overlapping parts of the 2 years' time series—a period of 53 days—was 1.5°C higher in 2006 than in 2004. However, global radiation was lower in 2006 than 2004 which we interpreted as evidence that cloud

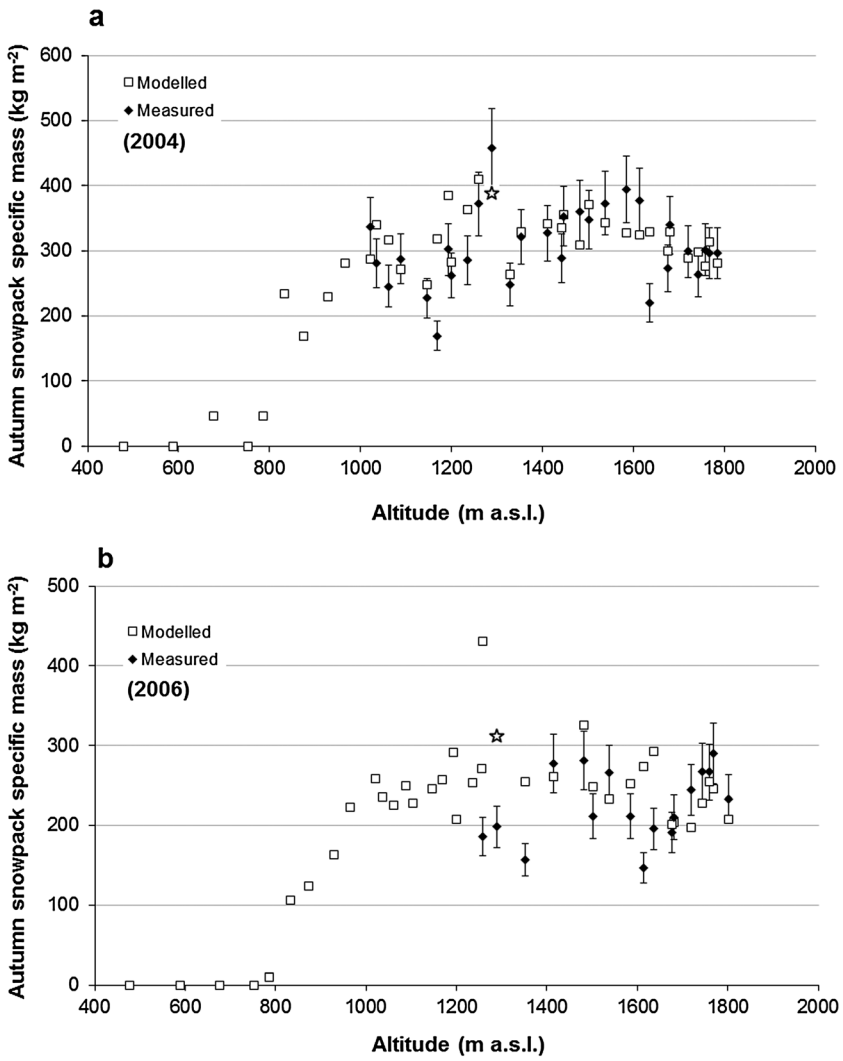

Figure 4. Measured and modeled values for autumn snowpack at all points down the transect for (a) 2004 water equivalent, (b) 2006 water equivalent, (c) 2004 surface height change, (d) 2006 surface height change, (e) 2004 bulk density, and (f) 2006 bulk density. Error bars on the measurements are based on kilometer-scale spatial variation, found from repeat measurements within 1 km scale nested grids. The modeled values at 1290 m asl, the position shown in Figure 9, are marked by stars.

cover was higher in 2006 than 2004. A higher value of *c* (50%) was therefore chosen to reflect these conditions, based on the expectation that across such a large highly reflective surface as the DIC, cloudier conditions would contribute to higher air temperatures. All other parameters were kept equal to the 2004 optimal parameter set run, to provide an appropriate validation of the model and the selected parameters.

Measurement sites used for both calibration and validation fall into DIC drainage basin 40 (Figure 1) as defined by *Burgess and Sharp* [2004] but do not include the lowest part of the basin. In order that whole-basin model results could be generated and compared to other studies, extra points were added to extend the model transect to sea level (with these extra points given the same density stratigraphy as the lowest measured point).

4.2. Sensitivity Testing

To gauge the sensitivity of melt-runoff relationships and the surface mass balance across the catchment to changes in the external and internal influences, the model runs for both years were repeated, with changes in the input data. Changes were made to the air temperature measurements used to drive the model, by adding/subtracting a set perturbation uniformly across the entire time series. Perturbations used for this purpose were up to ±2°C in both years. Separately, the depth of the impermeable layer within the firn was

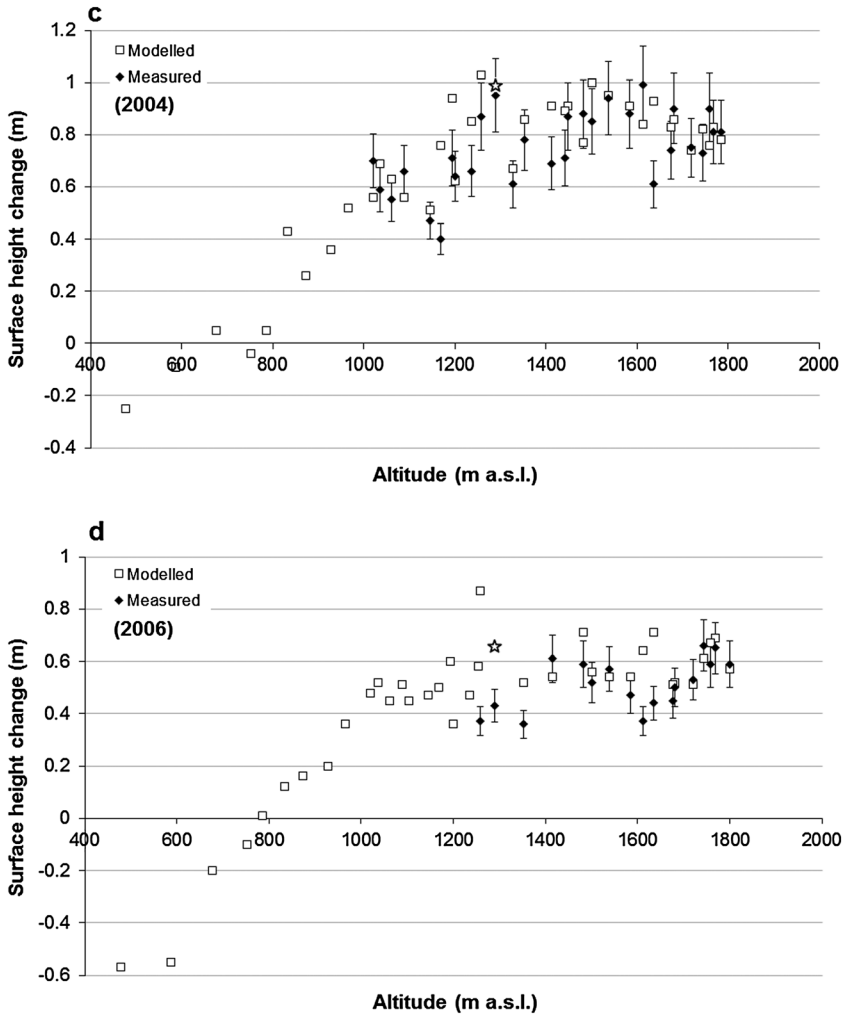

Figure 4. (continued)

also modified, by multiplying all the depth measurements by a set value. This method of modifying the depths was used so that the firn line remained at the same position on the transect. Values used varied between 0 (equivalent to placing the impermeable layer directly beneath the snowpack, at the annual layer) and 2 (a doubling of the impermeable layer depth).

5. Results

First, results at the point scale show the model's summer evolution of temperature and density profiles. Second, results on the scale of the measurement transect show the bulk snow and firn properties at each point and the location of transitions between accumulation zone snow facies. We compare model output with field measurements and observations. Knowing the ice cap hypsometry (e.g., Figure 1b), we distribute transect results across the catchment for easier comparison to other catchment-wide studies. Third, we show results from the sensitivity testing of the model to internal and external controls on the melt-runoff relationship and surface mass balance.

5.1. Point-Scale Results

At each point on the transect, seasonal evolution of temperature and density in the surface snowpack and underlying firn is modeled (shown in Figure 3 for a point at 1259 m asl). A time series of air temperature is shown in each year above the changing density and thermal structure of the snowpack. When the surface is heated, the warmth penetrates downward, while periods of lower surface temperature allow "cold content"

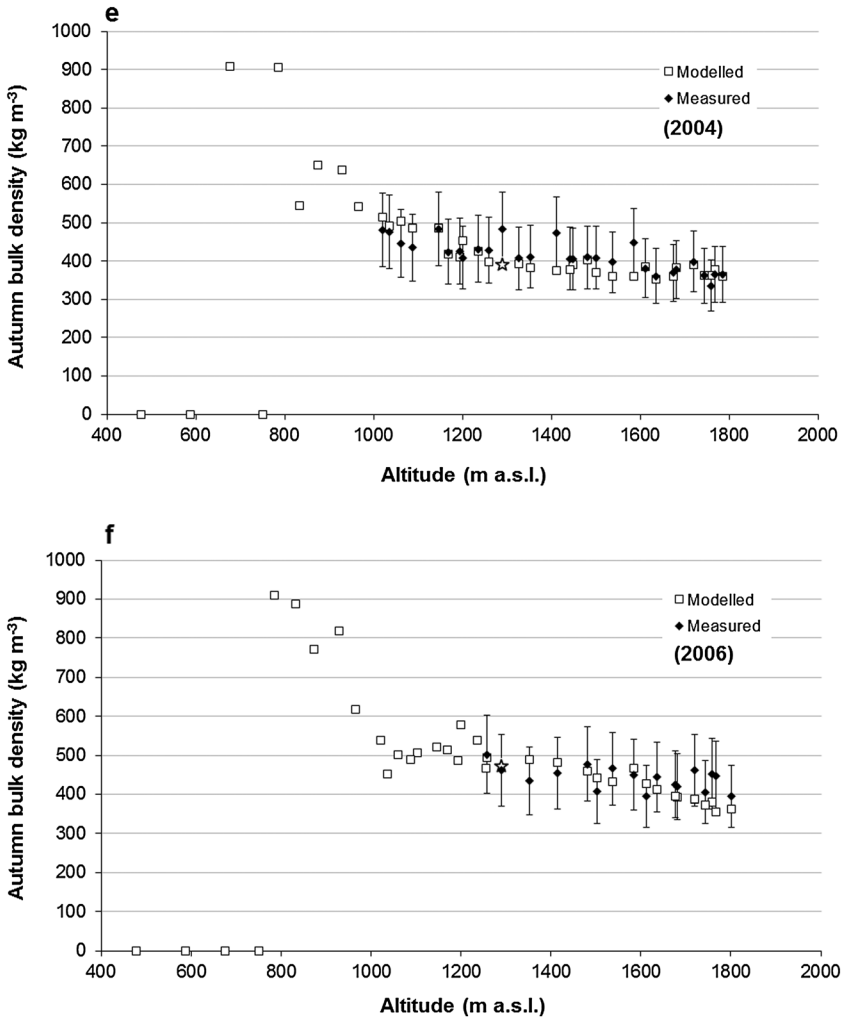

Figure 4. (continued)

to be conducted downward, cooling the near surface and causing net heat transfer to be upward. Melting occurs during warm periods, causing densification and ice layer formation at depths dependent on both density stratigraphy and thermal structure at the time of melting.

For example, in 2004 (Figure 3a), a dense layer begins to form in the snowpack at around 80 cm above the annual layer around day of year (DOY) 179, as air temperature begins to consistently hit daily maxima above 0°C and becomes steadily more established through time, reaching a density of around 700 kg m^{-3} by the end of the season. A second layer begins to establish a few centimeters above it on DOY 202, as air temperatures rise back above freezing after a 9 day colder period. DOYs 203 and 204 see meltwater reach its greatest depth below the surface, just 59 cm above the annual layer, causing a brief period of densification on both sides of a stratigraphic boundary there. The two main layers cease densification on DOY 212, the day on which regular daily maxima above freezing cease. Thereafter, melting and refreezing are restricted to the top few centimeters below the snow surface. The temperature evolution plot shows that the ice layer creation drives warming in the subsurface, which reaches a peak of warmth at the end of the period of ice layer formation. This is due to both the release of latent heat by the refreezing of meltwater and the concurrent high air temperatures.

5.2. Transect-Scale Results

Figure 4 shows the comparison between modeled and measured end-of-season bulk snowpack properties, at all points on the transect in both years, in terms of snowpack water equivalent, snowpack height, and snowpack bulk density. Root-mean-square difference (RMSD) values are shown in Table 2. Figure 5 shows the

Table 2. Modeled and Measured Autumn Bulk Properties Across All Measured Sites and the Root-Mean-Square Differences (RMSD) Between Them

Name	Symbol	Bounds	Step	Unit
Albedo (fresh snow)	α_s	0.76–0.88	0.015	
Albedo (ice)	α_i	0.41–0.65	0.03	
Density (fresh snow)	ρ_s	280–440	20	kg m^{-3}
Snow-rain threshold temperature		−0.5–1.9	0.3	°C
Cloud cover	c	0.1–0.9	0.1	

total amounts of melt, refreezing (within both the snowpack and the firn), and runoff in both years at all modeled points. Note that the totals are cumulative so that, e.g., the refreezing within the snowpack at the lower sites occurred early in the season, before subsequent removal of the snow and refrozen material. The model output allows the elevation of the wet snowline and the runoff line to be determined. The wet snowline is where percolating meltwater first warms the entire surface snowpack to the melting point and begins to percolate into the subsnowpack firn [*Benson*, 1962]. The runoff line is the location above which no meltwater runs off the ice cap. The modeled wet snowline can be compared with a measurement-based

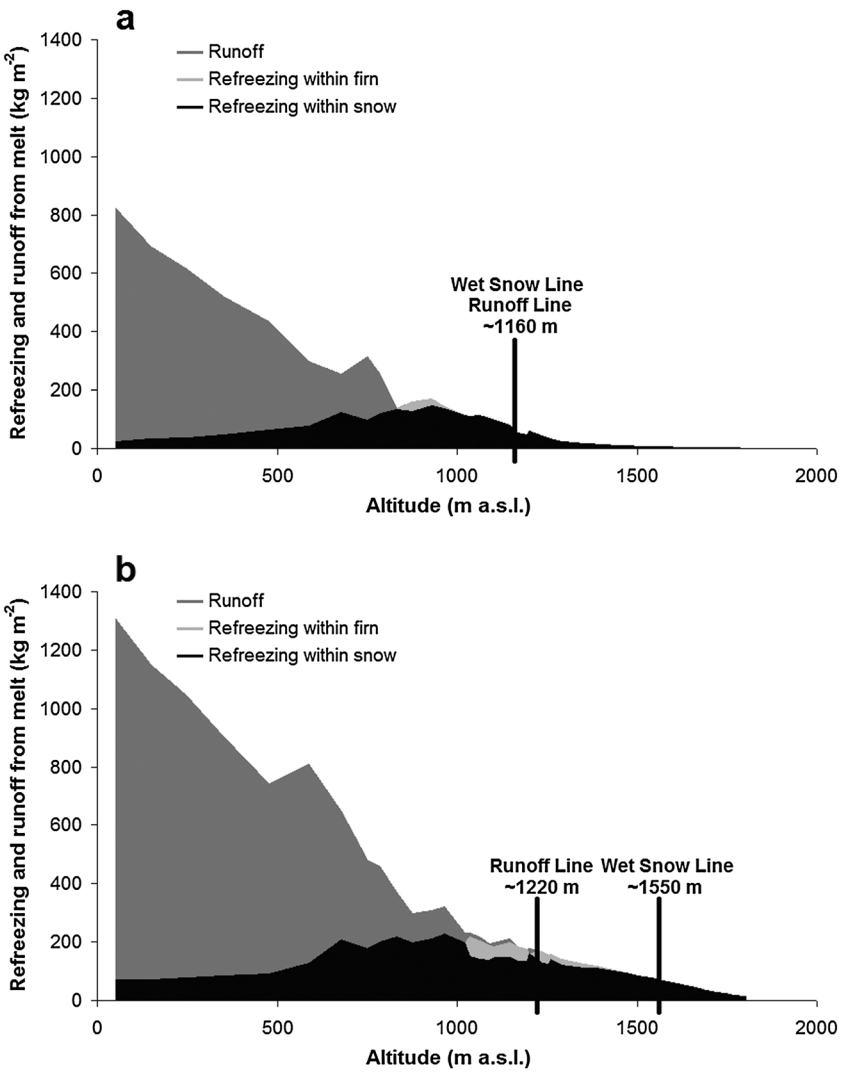

Figure 5. Modeled cumulative melt in terms of specific mass, split into a stacked area graph showing refreezing and runoff, across the transect for the (a) 2004 and (b) 2006 model runs. The altitudes of the wet snow and runoff lines are shown.

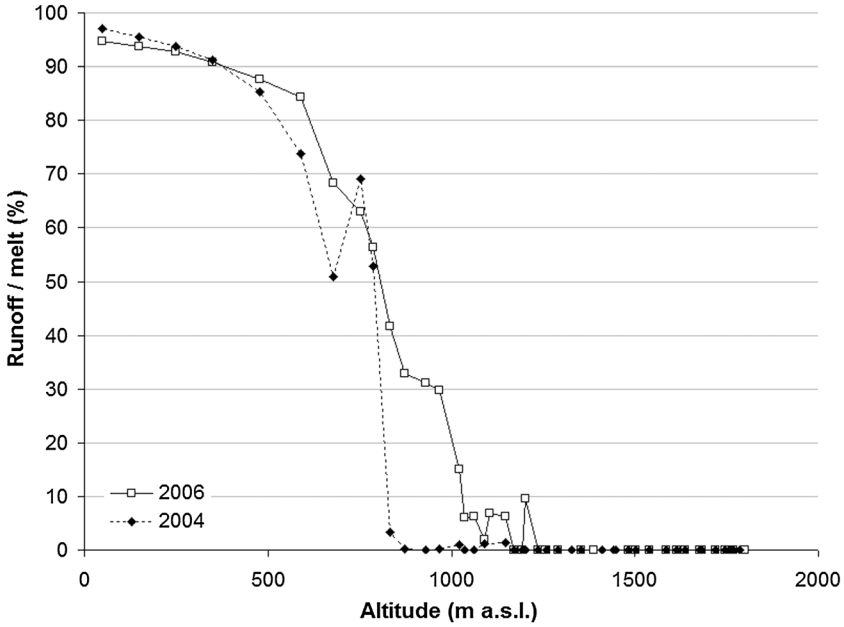

Figure 6. Percentage of melt becoming runoff at all points on the modeled transect.

estimate. The measurement-based values should be treated as minimum values, as heterogeneous percolation can lead to penetration of meltwater past the annual layer without densification of the snow immediately above it. Nevertheless, the wet snowline elevation found by the model is ~ 90 m lower than a measurement-based estimate in 2004, and ~ 140 m lower in 2006. The runoff line cannot be determined from our field measurements.

The model predicts that the fraction of melt that becomes runoff changes down the transect from 0% at the upper elevations to ~ 95% by sea level (Figure 6). The runoff line lies at ~1160 m asl in 2004 and ~1220 m asl in 2006. Surface mass balance curves that include internal accumulation were produced for both years (shown as the black, 0°C perturbation lines in Figure 8). Over the transect, 2006 is a generally less positive/more negative mass balance year. The equilibrium line altitude (ELA) in 2006 is ~780 m asl (to nearest 10 m). In 2004, it is possible to interpret two different figures for the ELA, the higher at ~770 m asl and the lower at ~640 m asl (to nearest 10 m). Using the catchment hypsometry (Figure 1b), the total melt and runoff for the 2004 and 2006 summers was calculated. The total modeled surface mass balance of the Croker Bay catchment for both years was +0.26 Gt in 2004 and +0.18 Gt in 2006.

5.3. Sensitivity Testing Results

The model sensitivity to impermeable layer depth was tested first. Very little change was discernible in both the melt-runoff relationship, and the surface mass balance found in both years when the impermeable layer depth within the firn was multiplied by values between 0 and 2, and the altitudes of the wet snow and runoff lines do not change from those shown in Figure 5. Also, the fraction of melt running off varies by less than 0.9% in 2004 and less than 1.2% in 2006. The surface mass balance is similarly unaffected, varying by less than 0.0008 Gt and 0.0043 Gt in 2004 and 2006, respectively. What small change does occur is as a result of the runoff increasing with a shallower impermeable layer and decreasing with a deeper impermeable layer. This causes the surface mass balance to slightly increase with increasing impermeable layer depth.

The model is much more sensitive to air temperature, as shown in Figure 7. For a negative air temperature perturbation, the runoff fraction of melt remains similar in both years. However, for a positive air temperature perturbation, the 2006 runoff fraction increases more steeply than the 2004 one (Figure 7a). This, of course, ignores any potential change in the melt-runoff relationship due to changes in other meteorological variables such as accumulation. The surface mass balance of the catchment is also highly sensitive to temperature (Figure 7b). The variation in surface mass balance in each year fits very closely to a parabolic curve.

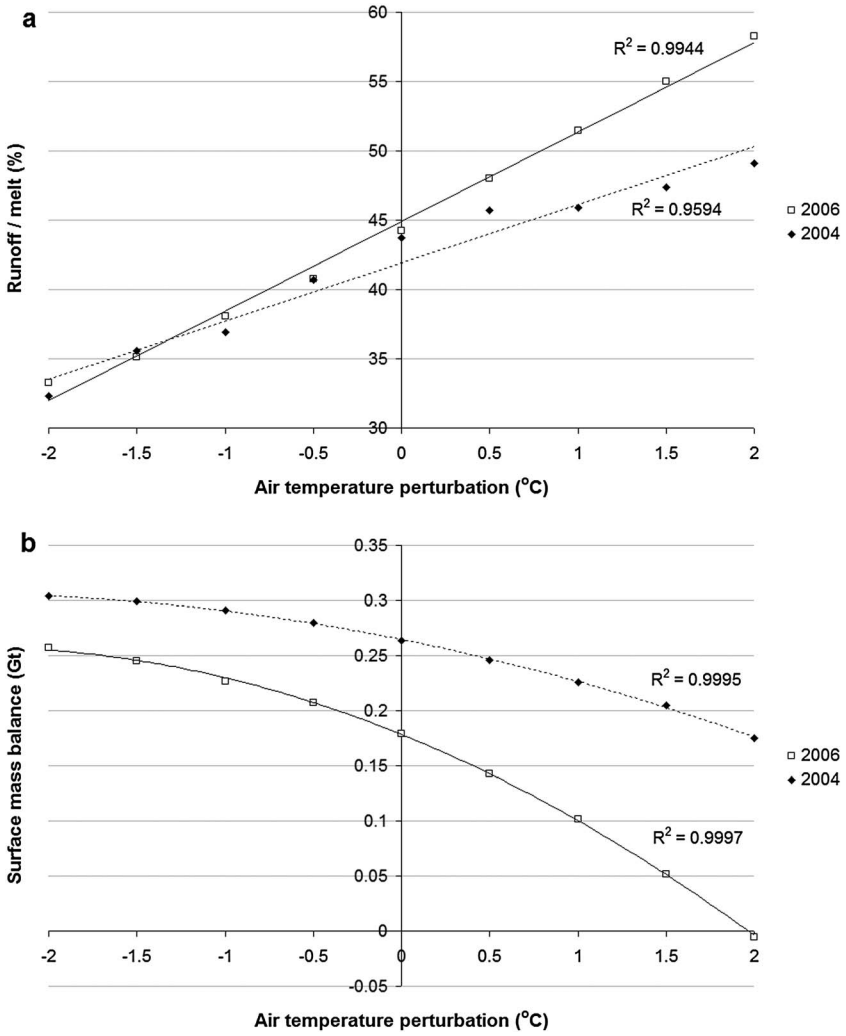

Figure 7. (a) Change in runoff as a fraction of melt and (b) change in surface mass balance, across the modeled catchment in both years, with change in air temperature.

Finally, surface mass balance curves for the perturbed model runs in both years are shown alongside the curves for the unperturbed runs in both years in Figure 8. In 2004 (Figure 8a) the equilibrium line shows a very small rise with temperature increase but a large lowering with lower temperatures. In 2006 (Figure 8b) the equilibrium line varies more linearly with altitude, and in this year the gradient of the trend line best fitting the relationship is 110 m °C^{-1} ($R^2 = 0.9832$).

6. Discussion

At any given point, the modeled autumn snowpack density profile is not ever likely to be an accurate representation of the autumn measurement. This is due to the simplification of small-scale processes in the model and the inability of kilometer-scale snowpit measurements to accurately reflect the complex reality of snowpack density structure. For example, repeat snowpit measurements at AWS sites reveals differences in percolation depths of many tens of centimeters over length scales of 10^0–10^3 m [*Bell*, 2008]. Nevertheless, a comparison of modeled and measured snowpack density profiles (e.g., Figure 9) indicates that most snowpack densification in reality occurs at greater depths than in the model. This is also evident in the model's apparent underestimate of the elevation of the wet snowline, although some difference between the modeled and measured values is to be expected as the wet snow "line" is really a broad zone of transition in snowpack processes. However, these comparisons suggest that the model has a strong tendency to refreeze percolating

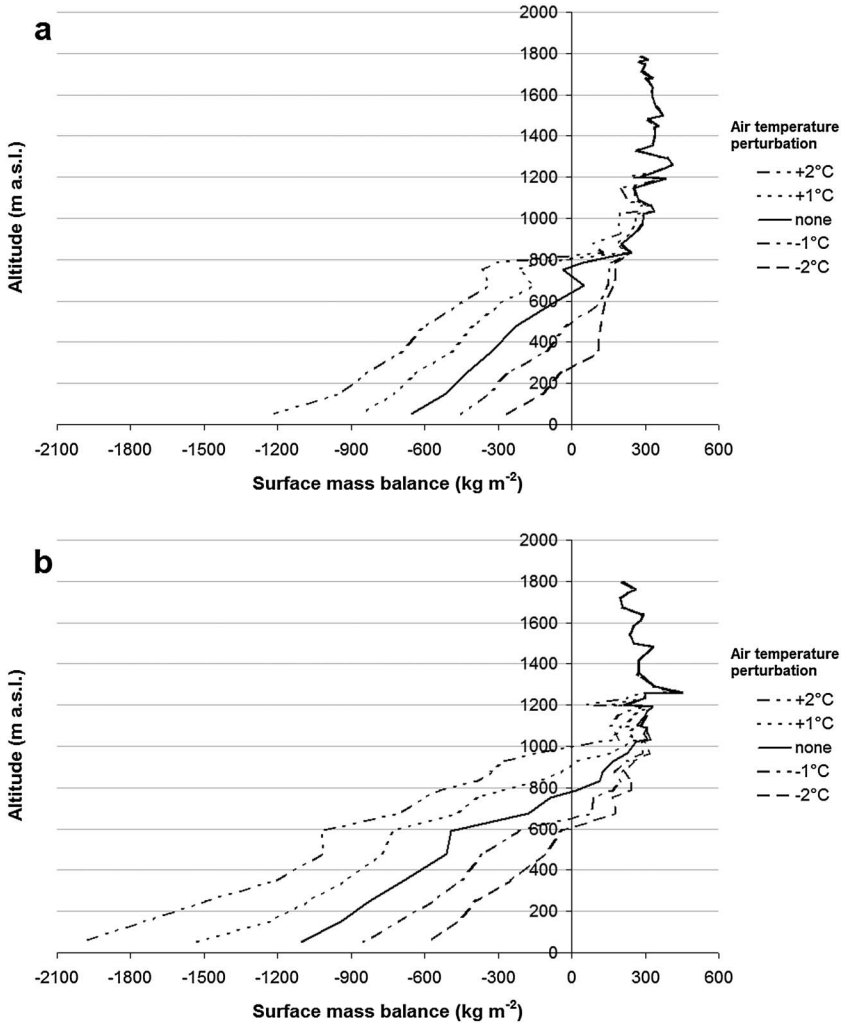

Figure 8. Modeled surface mass balance curves for various air temperature perturbations (°C), in (a) 2004 and (b) 2006. "None" (solid line) in both graphs are the runs without perturbation, described in Figures 4–7.

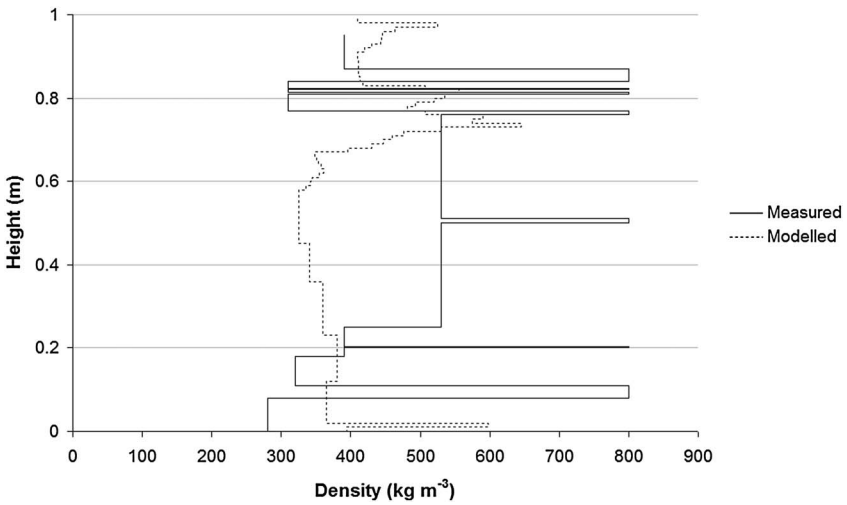

Figure 9. Measured and modeled autumn snowpack density profiles at 1290 m asl in 2004.

meltwater at shallower depths than are seen in reality. Without some treatment of finger-flow percolation the model is unlikely to be effective at characterizing the snowpack stratigraphy at any given location. In addition, the model does not include the effects of the lateral transfer of percolating meltwater which was clearly evident in 2006, below around 1350 m asl as surface runoff within a saturated snowpack [*Bell et al.*, 2008, Figure 7, p. 163]. It may simply not be possible to match measurements with model output at the point scale. *Obleitner and Lehning* [2004], using a more detailed model, found that it too could not reproduce stratigraphic detail [*Obleitner and Lehning,* 2004, Figure 7b] but that it replicated the bulk density well. Being able to match trends in the bulk measurements across the transect is therefore perhaps a much more realistic goal for the model than matching measurements at the point scale. In this respect our model does well, and trends in bulk snowpack measurements (snow depth, average snow density, and snowpack water equivalent) are generally matched by the model at the transect scale (Figure 4).

Colgan and Sharp [2008] found using firn cores that the 1989–2003 average elevation of the dry snowline lay above the ice cap summit. Our model found melt at all sites on the transect, meaning that the modeled dry snowline was also above the ice cap summit (though in 2004 modeled melt in the upper transect was very low, dropping to < 3 kg m^{-2} at the sites above 1700 m asl.).

A broad transition zone found by the model, between the area where no melt runs off and the area where a very high fraction of melt runs off (Figure 6) is in agreement with other studies. *Humphrey et al.* [2012] found that this transition zone is ~20 km wide on the Greenland Ice Sheet, ranging between ~1500 and ~1350 m asl. This study finds a narrower transition zone on DIC, up to 14 km wide, but covering a larger elevation range of ~300 m. We also find that the width and elevation range of the transition zone is variable between years and depends on the definition of the "all runoff" zone, since even at low altitudes a small amount of refreezing can occur early in the melt season while the snowpack remains cold.

The transect-scale results show that the model finds the equilibrium line to lie at similar altitudes in the two modeled years, despite quite different meteorological conditions (Figure 8) and quite different overall catchment surface mass balance (SMB) values. Although the ELA generally rises and falls with a decrease and increase in surface mass balance, respectively, this is not always the case since the depth, structure, and thermal regime of the near-surface firn play an important role in determining the extent to which surface melt refreezes or becomes runoff [*Koerner*, 1970]. The effect of the underlying firn on refreezing and surface mass balance profiles is developed further below in relation to the results from sensitivity testing, but it is worth highlighting that the sensitivity of the ELA to air temperature is partly a function of meteorological conditions during the preceding years.

The model suggests that the runoff/melt ratio and the surface mass balance are quite insensitive to the impermeable layer depth. This result is caused by the relationship between refreezing within the firn and that occurring within the annual snowpack. When the impermeable layer is placed at shallower depths, the decrease in refreezing within the firn is not simply equalled by an increase in surface runoff but is partly compensated for by an increase in refreezing within the annual snowpack. This is because the heat supply provided by the refreezing within the firn, which would be conducted up into the snowpack to lower the cold content there, is removed. The refreezing capacity of the annual snowpack is thus increased.

Both years show a parabolic decrease in surface mass balance with increasing air temperature (Figure 7b) which partly reflects the catchment hypsometry. Most of the catchment is located above 1000 m, so a larger area of the catchment experiences melt and runoff as air temperature rises. However, the sensitivity of the SMB and ELA to temperature rises is quite different in the 2 years. The 2004 runs with increased air temperature cause a large increase in the amount of refreezing within the firn just above the equilibrium line (up to 4.5 times for the "+2°C" run compared to the run without perturbation), suggesting that the presence of the firn is mitigating the increase in air temperatures. The refreezing within the firn in 2006 does not increase with air temperature to the same extent as in 2004, with the refreezing around the equilibrium line increasing by a factor of less than 2 between the unperturbed run and the "+2°C" one. This is due to the firn in 2006 being already warmer when meltwater reaches it, and the greater amounts of refreezing in the "standard" run to begin with. The reduction of refreezing capacity of warmer firn provides an accelerator in the relationship between increasing air temperatures and increasing runoff when high air temperatures are sustained from 1 year to the next.

An investigation into the future sensitivity of the Greenland Ice Sheet to rising air temperatures throughout the 21st century was undertaken by *Van Angelen et al.* [2013]. This study coupled a snowpack/firn evolution model with a regional climate model to show that the refreezing capacity of the firn across Greenland would reduce with sustained rising air temperatures. Although recognizing the importance of warmer firn temperatures, they proposed that the primary mechanism for reduced refreezing capacity was a long-term reduction in pore space in the firn. Our sensitivity analyses support this general conclusion, but our modeled surface mass balance is more sensitive to the temperature of the winter snowpack and firn than to the pore space available for refreezing in the firn (which in our experiments is effectively controlled by the depth of the impermeable layer).

The sensitivity of the mass balance of the entire Canadian Arctic Archipelago to air temperature change was found by *Gardner et al.* [2011] to be -430 kg m^{-2} a^{-1} K^{-1}. Figure 7 shows that the sensitivity itself increases with a period of sustained increasing temperature. This effect may account for the extremely high rates of mass loss observed across DIC and other ice masses in the Canadian High Arctic during the period 2005–2009 [*Sharp et al.*, 2011], which was characterized by a succession of warm summers.

The unperturbed runs give values for the catchment surface mass balance of +0.26 Gt in 2004 and +0.18 Gt in 2006. These compare well with the average rate of $+0.15 \pm 0.05$ Gt a^{-1} between 1963 and 2000 determined using measurements of surface mass balance across the accumulation area by *Mair et al.* [2005]. In agreement with the latter, *Burgess and Sharp* [2004] found that the catchment increased slightly in area between 1960 and 2000. However, the model predicts that all else being equal, the mass balance of the catchment becomes negative for air temperatures around 2°C higher than those measured in 2006.

7. Conclusions

We modify an existing physically based snow and firn model to increase vertical resolution of snow and firn temperature and density evolution throughout a summer melt season. We apply the model to a transect of Devon Ice Cap to investigate the relationship between melt, refreezing, and runoff and the distributions of surface snow facies along a ~45 km transect of the ice cap. Uniquely, our model is initialized, calibrated, and validated with high-resolution field measurements including snowpack stratigraphies before and after summer melt in two melt seasons, at kilometer-scale spatial resolution along the transect. By calculating the evolution of the density stratigraphy and thermal profile at each point on the transect over the melt season, the model determines final snowpack properties. Model runs were carried out for the 2004 and 2006 seasons down the full measured transect. Model output from these runs was compared with autumn measurements.

The model produces values for melt, refreezing within the snow and firn, and runoff at each point for which it is run. These are used to calculate altitudes for the wet snowline and runoff line, and for the equilibrium line including the effects of internal accumulation. The model does a good job of matching the along-transect trend of bulk snowpack variables, such as depth, density, and water equivalent and is capable of identifying the broad transition zones between different surface snow facies. Successfully modeling snow facies boundaries is beneficial to the process of retrieving the ice cap surface elevations from radar backscatter returns [*Scott et al.*, 2006]. Knowledge of how the bulk snowpack characteristics change through space and time could provide the basis for development of an empirical correction to radar altimetry-derived surface estimates [*Thomas et al.*, 2008] or could be used to select the most appropriate surface retracker algorithm according to the changing snow facies [*Ferraro and Swift*, 1995; *Helm et al.*, 2007]. Our model cannot replicate measured snowpack density stratigraphies at the point scale and underestimates the quantity of meltwater percolation into the firn below the wet snowline. This suggests that the processes governing percolation are inadequate, and modifications to simulate finger-flow percolation of surface generated meltwater should be considered.

Much more melt and runoff occur in 2006 than 2004, but the ratio of runoff to melt in the 2 years is similar. Although the modeled mass balance is positive in both years, it is much higher in 2004 than 2006. Previous work suggests that the catchment had a positive mass balance up to 2000, and our results suggest that this continued up to 2006. Very high melt rates have been measured across DIC in the years from 2006 to 2012 which have resulted in a significant densification of the near-surface firn [*Bezeau et al.*, 2013]. Increased mass loss from the ice caps of the Canadian Arctic Archipelago (CAA) have been recorded during this period and argued to be mainly due to increased meltwater runoff due to elevated summer air temperatures [*Gardner et al.*, 2011]. This finding was in part based upon the application of a temperature index melt model with a modified meltwater retention scheme to annual snowpacks. The development of a spatially distributed version of our

model across the DIC and other ice caps within the CAA will better determine the contribution of meltwater runoff to mass loss during the period 2006–2012.

The sensitivity of the model to both internal and external controls was tested by separately varying the impermeable layer depth and air temperature. The model is insensitive to variations in impermeable layer depth, as change in refreezing within the firn is mitigated by an opposite change in refreezing within the snow, due to the thermal connection between the two. The model is, however, highly sensitive to change in air temperature, which changes the fraction of melt that becomes runoff and causes a parabolic change in catchment surface mass balance. Change in the ELA in 2004 for a rise in air temperature is small as the firn around the ELA is able to refreeze much of the extra meltwater. However, in 2006 the warmer conditions cause the capacity of the snow and firn around the ELA to be exceeded quickly, and therefore, the ELA rises much more quickly with temperature increase.

The effects of increased runoff/melt ratio and reduced refreezing capacity with increasing temperature could cause a significant accelerator in the relationship between runoff and air temperature if high temperatures are sustained for several years. Model-based projections of future surface mass balance that take this effect into account will provide more robust estimates of the sensitivity of ice masses to air temperature rises. A wider application of a distributed version of our model will (a) contribute toward a better assessment of the mass loss sensitivity of the ice caps of the CAA and other ice masses to future climate change scenarios and (b) help identify the relative importance of long-term changes in subsurface thermal and structural (density) regimes to this sensitivity.

Acknowledgments

R.M.M. was supported by the Scottish Alliance for Geoscience, Environment and Society (SAGES). The field data collection contributed to the validation of the European Space Agency Cryosat mission and was supported by the Natural Sciences and Engineering Research Council, Canada, the Meteorological Service of Canada (CRYSYS program), the Polar Continental Shelf Project (an agency of Natural Resources Canada), and by UK Natural Environment Research Council consortium grant NER/O/S/2003/00620. Support for D.O.B. was provided by the Canadian Circumpolar Institute and the Climate Change Geoscience Program, Earth Sciences Sector, Natural Resources Canada (ESS contribution 20130371). Thanks are also due to the Nunavut Research Institute and the communities of Resolute Bay and Grise Fjord for permission to conduct fieldwork on Devon Ice Cap. M.J. Sharp, A. Gardner, F. Cawkwell, R. Bingham, S. Williamson, L. Colgan, J. Davis, B. Danielson, J. Sekerka, L. Gray, and J. Zheng are thanked for logistical support and field assistance during the data collection. We thank Ruzica Dadic, two other anonymous reviewers, and the Editor, Bryn Hubbard, for their helpful comments on an earlier version of this paper and which resulted in significant improvements.

References

Bassford, R. (2002), Geophysical and numerical modelling investigations of the ice caps on Severnaya Zemlya, PhD thesis, University of Bristol, U. K.

Bassford, R., M. Siegert, and J. Dowdeswell (2006), Quantifying the mass balance of ice caps on Severnaya Zemlya, Russian High Arctic 1: Climate and mass balance of the Vavilov Ice Cap, *Arct. Antarct. Alp. Res.*, *38*(1), 1–12.

Bell, C. (2008), Controls on spatial and temporal variability in the snowpack of a high Arctic ice cap: The Devon Island Ice Cap, Nunavut, Canada, PhD thesis, University of Aberdeen, U. K.

Bell, C., D. Mair, D. Burgess, M. Sharp, M. Demuth, F. Cawkwell, R. Bingham, and J. Wadham (2008), Spatial and temporal variability in the snowpack of a High Arctic ice cap: Implications for mass-change measurements, *Ann. Glaciol.*, *48*, 159–170.

Benson, C. (1962), Stratigraphic studies in the snow and firn of the Greenland Ice Sheet, *CRREL Res. Rep. 70*.

Bezeau, P., M. Sharp, D. Burgess, and G. Gascon (2013), Firn profile changes in response to extreme 21st-century melting at Devon Ice Cap, Nunavut, Canada, *J. Glaciol.*, *59*(217), 981–991.

Bougamont, M., J. L. Bamber, J. K. Ridley, R. M. Gladstone, W. Greuell, E. Hanna, A. J. Payne, and I. Rutt (2007), Impact of model physics on estimating the surface mass balance of the Greenland Ice Sheet, *Geophys. Res. Lett.*, *34*, L17501, doi:10.1029/2007GL030700.

Brandt, R., and S. Warren (1993), Solar-heating rates and temperature profiles in Antarctic snow and ice, *J. Glaciol.*, *39*(131), 99–110.

Brathwaite, R., M. Latersner, and W. T. Pfeffer (1994), Variations of near-surface firn density in the lower accumulation area of the Greenland ice sheet, Pakitsoq, West Greenland, *J. Glaciol.*, *40*(136), 477–485.

Brutsaert, W. (1975), On a derivable formula for long-wave radiation from clear skies, *Water Resour. Res.*, *11*(5), 742–744, doi:10.1029/WR011i005p00742.

Bugnion, V., and P. Stone (2002), Snowpack model estimates of the mass balance of the Greenland ice sheet and its changes over the twenty-first century, *Climate*, *20*(1), 87–106.

Burgess, D., and M. Sharp (2004), Recent changes in areal extent of the Devon Ice Cap, Nunavut, Canada, *Arct. Antarct. Alp. Res.*, *36*(2), 261–271.

Campbell, F., P. Nienow, and R. Purves (2006), Role of the supraglacial snowpack in mediating meltwater delivery to the glacier system as inferred from dye tracer investigations, *Hydrol. Processes*, *20*(4), 969–985.

Colbeck, S., E. Akitaya, R. Armostrong, H. Gubler, J. Lafeuille, K. Lied, D. McClung, and E. Morris (1990), The international classification for seasonal snow on the ground, The International Commission on Snow and Ice of the International Association of Scientific Hydrology.

Colgan, W., and M. Sharp (2008), Combined oceanic and atmospheric influences on net accumulation on Devon Ice Cap, Nunavut, *Can. J. Glaciol.*, *54*(184), 28–40.

Ferraro, E. J., and C. T. Swift (1995), Measuring geophysical parameters of the Greenland ice sheet using airborne radar altimetry, *J. Glaciol.*, *41*(139), 607–618.

Gardner, A., G. Molholdt, B. Wouters, G. Wolken, D. Burgess, M. Sharp, J. G. Cogley, C. Braun, and C. Labine (2011), Sharply increased mass loss from glaciers and ice caps in the Canadian Arctic Archipelago, *Nature*, *473*, 357–360.

Greuell, W., and T. Konzelmann (1994), Numerical modelling of the energy balance and the englacial temperature of the Greenland Ice Sheet. Calculations for the ETH-Camp location (West Greenland, 1155 m a.s.l.), *Global Planet. Change*, *9*(1–2), 91–114.

Harper, J. T., and J. H. Bradford (2003), Snow stratigraphy over a uniform depositional surface: Spatial variability and measurement tools, *Cold Reg. Sci. Technol.*, *37*, 289–298.

Helm, V., W. Rack, R. Cullen, P. Nienow, D. Mair, V. Parry, and D. J. Wingham (2007), Winter accumulation in the percolation zone of Greenland measured by airborne radar altimeter, *Geophys. Res. Lett.*, *34*, L06501, doi:10.1029/2006GL029185.

Herron, M., and C. Langway (1980), Firn densification: An empirical model, *J. Glaciol.*, *25*(93), 373–385.

Hock, R. (2005), Glacier melt: A review of processes and their modelling, *Prog. Phys. Geogr.*, *29*(3), 362–391.

Humphrey, N. F., J. T. Harper, and W. T. Pfeffer (2012), Thermal tracking of meltwater retention in Greenland's accumulation area, *J. Geophys. Res.*, *117*, F01010, doi:10.1029/2011JF002083.

Janssens, I., and P. Huybrechts (2000), The treatment of meltwater retention in mass-balance parameterizations of the Greenland Ice Sheet, *Ann. Glaciol.*, *31*, 133–140.
Koerner, R. (1970), The mass balance of the Devon Island ice cap, Northwest Territories, Canada, 1961–66, *J. Glaciol.*, *9*(57), 325–336.
Kustas, W., A. Rango, and R. Uijlenhoet (1994), A simple energy budget algorithm for the snowmelt runoff model, *Water Resour. Res.*, *30*(5), 1515–1527, doi:10.1029/94WR00152.
Mair, D., D. Burgess, and M. Sharp (2005), Thirty-seven year mass balance of Devon Ice Cap, Nunavut, Canada, determined by shallow ice coring and melt modeling, *J. Geophys. Res.*, *110*, F01011, doi:10.1029/2003JF000099.
Meehl, G., et al. (2007), Global climate projections, in *Climate Change 2007: The Physical Science Basis. Contribution of Working Group I to the Fourth Assessment Report of the Intergovernmental Panel on Climate Change*, edited by S. Solomon et al., chap. 10, Cambridge Univ. Press, Cambridge, U. K. and New York.
Obleitner, F., and M. Lehning (2004), Measurement and simulation of snow and superimposed ice at the Kongsvegen glacier, Svalbard (Spitzbergen), *J. Geophys. Res.*, *109*, D04106, doi:10.1029/2003JD003945.
Oerlemans, J. (1992), Climate sensitivity of glaciers in southern Norway: Application of an energy-balance model to Nigardsbreen, Hellstugubreen and Alfotbreen, *J. Glaciol.*, *38*(129), 223–232.
Partington, K., J. Ridley, and C. Rapley (1989), Observations of the surface properties of the ice sheets by satellite radar altimetry, *J. Glaciol.*, *35*(120), 267–275.
Paterson, W. (1994), *The Physics of Glaciers*, 3rd ed., Butterworth-Heinemann, Oxford.
Pfeffer, W., M. Meier, and T. Illangasekare (1991), Retention of Greenland runoff by refreezing: Implications for projected future sea level change, *J. Geophys. Res.*, *96*(C12), 22,117–22,124, doi:10.1029/91JC02502.
Reeh, N., D. Fisher, R. Koerner, and H. Clausen (2005), An empirical firn-densification model comprising ice lenses, *Ann. Glaciol.*, *42*, 101–106.
Reijmer, C. H., M. R. van den Broeke, X. Fettweis, J. Ettema, and L. B. Stap (2012), Refreezing on the Greenland ice sheet: A comparison of parameterizations, *Cryosphere*, *6*, 743–762.
Scott, J., P. Nienow, D. Mair, E. Morris, and D. Wingham (2006), Importance of seasonal and annual layers in controlling backscatter to radar altimeters across the percolation zone of an ice sheet, *Geophys. Res. Lett.*, *33*, L24502, doi:10.1029/2006GL027974.
Sharp, M., D. O. Burgess, J. G. Cogley, M. Ecclestone, C. Labine, and G. J. Wolken (2011), Extreme melt on Canada's Arctic ice caps in the 21st century, *Geophys. Res. Lett.*, *38*, L11501, doi:10.1029/2011GL047381.
Thomas, R., C. Davis, E. Frederick, W. Krabill, Y. Li, S. Manizade, and C. Martin (2008), A comparison of Greenland ice-sheet volume changes derived from altimetry measurements, *J. Glaciol.*, *54*(185), 203–212.
Van Angelen, J. H., J. T. M. Lenaerts, M. R. van den Broeke, X. Fettweis, and E. van Meijgaard (2013), Rapid loss of firn pore space accelerates 21st century Greenland mass loss, *Geophys. Res. Lett.*, *40*, 2109–2113, doi:10.1002/grl.50490.
Van den Broeke, M., P. Smeets, J. Ettema, C. van der Veen, R. van de Wal, and J. Oerlemans (2008), Partitioning of melt energy and meltwater fluxes in the ablation zone of the west Greenland ice sheet, *Cryosphere*, *2*, 179–189.
Wright, A. (2005), The impact of meltwater refreezing on the mass balance of a High Arctic Glacier, PhD thesis, University of Bristol, U. K.
Wright, A., J. Wadham, M. Siegert, A. Luckman, and J. Kohler (2005), Modelling the impact of superimposed ice on the mass balance of an Arctic glacier under scenarios of future climate change, *Ann. Glaciol.*, *42*, 277–283.
Wright, A., J. Wadham, M. Siegert, A. Luckman, J. Kohler, and A. Nuttall (2007), Modeling the refreezing of meltwater as superimposed ice on a high Arctic glacier: A comparison of approaches, *J. Geophys. Res.*, *112*, F04016, doi:10.1029/2007JF000818.
Zwally, J., and J. Li (2002), Seasonal and interannual variations of firn densification and ice-sheet surface elevation at the Greenland summit, *J. Glaciol.*, *48*(161), 199–207.